THE JOURNAL OF PHYSICAL CHEMISTRY B

Article

Cite This: J. Phys. Chem. B 2019, 123, 5730−5741

pubs.acs.org/JPCB

Untangling Hydrogen Bond Networks with Ion Mobility Spectrometry and Quantum Chemical Calculations: A Case Study on H^+XPGG

Daniel Beckett, Tarick J. El-Baba, Kevin Gilbert, David E. Clemmer, and Krishnan Raghavachari*

Department of Chemistry, Indiana University, Bloomington Indiana 47401, United States

Supporting Information

ABSTRACT: Ion mobility spectrometry-mass spectrometry and quantum chemical calculations are used to determine the structures and stabilities of singly protonated XaaProGlyGly peptides: H^+DPGG, H^+NPGG, H^+EPGG, and H^+QPGG. The IMS distributions are similar, suggesting the peptides adopt closely related structures in the gas phase. Quantum chemical calculations show that all conformers seen in the experimental spectrum correspond to the *cis* configuration about the Xaa−Pro peptide bond, significantly different from the behavior seen previously for H^+GPGG. Density functional theory and quantum theory of atoms in molecules (QTAIM) investigations uncover a silent drama as a minor conformer not observed in the H^+DPGG spectrum becomes the preferred conformer in H^+QPGG, with both conformers being coincident in collision cross section. Investigation of the highly coupled hydrogen bond network, replete with CH···O interactions and bifurcated hydrogen bonds, reveals the cause of this effect as well as the absence of *trans* conformers from the spectra. A series of generalized observations are provided to aid in enzyme and ligand design using these coupled hydrogen bond motifs.

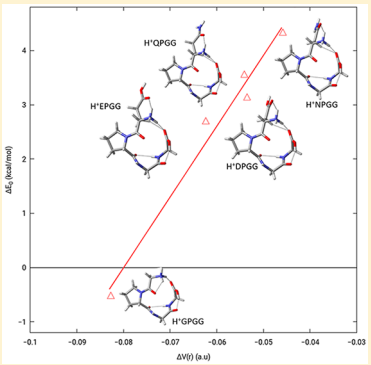

1. INTRODUCTION

Peptides and proteins are vital biomolecules responsible for carrying out biological functions, and they are known to exist in structural ensembles separated by low-energy barriers. Typically, the low energetic "native" structure is thought to be the only biologically active state, although functioning proteins with flexible or poorly defined structures challenge this paradigm. The ensemble nature of these peptides impedes our ability to predict their structures, especially when considering biomolecules which bear regions with intrinsic disorder.[1,2] Experimental tools such as X-ray crystallography[3] and nuclear magnetic resonance spectroscopy[4] can map the atomistic positions for well-structured polypeptides with extraordinary detail. However, these studies are difficult when investigating highly dynamic systems that diffract poorly or undergo rapid structural interconversions. As biomolecular function is intimately linked to structure,[1] there is an imminent need to devise new approaches to reveal how structure is established.

In some cases, single amino acid mutations can induce slight structural perturbations resulting in the buildup of toxic species. For example, β-2 microglobulin is a small protein serving as the light chain of the major histocompatibility class I complex responsible for activating T cells in acquired immune responses.[5−7] The mutation D76N on β-2 microglobulin causes it to aggregate, triggering the buildup of toxic amyloid fibrils. However, Asp to Asn mutations at the other seven positions (sites 34, 38, 53, 59, 76, 96, and 98) are not involved in amyloidosis.[7] The crystal structures for several of these species showed similarities in the overall fold as well as in the hydrogen bonding network near Asp76 except for D76N itself, which shows more rigid hydrogen bonds. This suggests that Asp confers more than just a negative charge to enhance stability and prevent fibril formation, highlighting the importance of understanding the effects of perturbing protein hydrogen bond networks.

While the conformers proteins adopt are influenced by a number of factors, the importance of hydrogen bonding in determining the structure of the dominant conformer should not be overlooked.[8−10] Even weak hydrogen bonds such as CH···O interactions have been found as a repeating motif in biological structures.[11,12] Bifurcated hydrogen bonds that share a single donor or acceptor (also referred to as three-center hydrogen bonds) have also been found in a number of species including DNA oligomers.[13,14] Specifically, in the case of enzymes, the structure and coupling of complex hydrogen bonding networks formed from bifurcated hydrogen bonds has been found to play a large role in the function of active sites, with recent experimental and computational work focused on the magnitude of such couplings.[15,16] However, these systems, being biologically relevant and active, are extremely complex: though bifurcated hydrogen bonds were found and observed to be coupled, little has been said in the way of general empirical rules on how the coupling of hydrogen bonds affects the

Received: April 23, 2019
Revised: June 4, 2019
Published: June 26, 2019

DOI: 10.1021/acs.jpcb.9b03803
J. Phys. Chem. B 2019, 123, 5730−5741

prevalence of certain structures or conformers. Herein we use ion mobility spectrometry and quantum chemical calculations to explore four model, singly protonated peptides, H^+XPGG, X being D, N, E, and Q, with the aim of understanding how simple, single-site mutations affect hydrogen bond networks and influence the preferred gas-phase conformer[17−19] of each specimen.

A number of groups are now using ion mobility spectrometry-mass spectrometry (IMS-MS) to study biomolecular structure and dynamics.[20−28] In IMS, the unique ion mobilities are determined by measuring the time required to traverse a drift tube filled with an inert buffer gas. The mobility measurements can be related to the ions' orientationally averaged collision cross section, which effectively reports on an ion's shape.[29] The solvent-free nature of gaseous ions prevents further structural interconversions that require interaction with bulk solvent.

IMS-MS techniques have recently been used to follow structural transitions of peptides and proteins.[21,25,28,30−34] However, IMS measurements rely on molecular dynamics simulations and quantum chemical calculations to glean insight into the atomic positions of the underlying structures.[35−38] We have previously benchmarked a wide variety of computational techniques on IMS measurements of H^+GPGG and will now interrogate the structures of conformers rather than assessing the accuracy of theory.[37] To assess the relative strengths of hydrogen bonds in each peptide conformer, we will employ the technique of Quantum Theory of Atoms in Molecules (QTAIM)[39−42] as well as general observations of hydrogen bond lengths and angles. QTAIM has been used widely in the study of hydrogen bonds,[42−49] including CH···O hydrogen bonds[50,51] and intramolecular three-centered (bifurcated) hydrogen bonds,[52] making it a desirable method to carry out the analysis in this work. QTAIM will be used here to verify the existence of hydrogen bonding interactions as well as assessing the potential energy densities at bond critical points as a measure of hydrogen bond strength.[47,49,50]

Herein we show the details of hydrogen bond coupling in the hairpin tetrapeptides H^+DPGG, H^+NPGG, H^+EPGG, and H^+QPGG. The hydrogen bond networks are only slightly perturbed by changes in the N-terminal residue, ensuring that all changes in the conformational landscape are due to hydrogen bonding, making these excellent test systems. The first section of Results and Discussion details the ion mobility spectra of all species and the conformers constituting the experimental spectra ascertained through high-level quantum chemical calculations. From here, we will relate the absence of *trans* conformers (about the Xaa−Pro peptide bond) in the spectra to the relative strengthening of the *cis* hydrogen bonding network as substitution occurs at the N-terminus. We will explain the effects of substituting D with N and E with Q as well as the effects of substituting D with E and N with Q on the hydrogen bonding network in the *cis* conformers. This analysis will demonstrate how a minor conformer in H^+DPGG becomes the dominant conformer in H^+QPGG due to a slight difference in the hydrogen bonding network exacerbated by the mutation to H^+QPGG. These results detail a case study with a number of lessons applicable to the fields of protein engineering and ligand design, illustrating often overlooked facets of hydrogen bonding networks in peptides.

2. METHODS

2.1. Computational Details. Conformers for each peptide were generated in the same manner as in our previous work on H^+GPGG.[37] Starting structures for each peptide were built in a β-strand configuration with PCMODEL.[53] Conformers were generated by stochastically rotating the rotatable bonds, quenching with the MMFF94 force field,[54] and discarding structures outside of a 7 kcal/mol energy window. Generated conformers were optimized with the PM6 semiempirical method[55] as implemented in Gaussian 16,[56] and degenerate structures were discarded. Conformers were further optimized, and frequencies obtained, with the CAM-B3LYP-D3BJ/6-311++G(d,p) level of theory,[57−64] which was found to produce intensities closest to both experiment and CCSD(T)/CBS calculations in our previous work.[37] All structures were verified to be minima by frequency calculations, and thermochemical properties were obtained within the rigid rotor/harmonic oscillator approximation.[56]

Collision cross sections were obtained via the trajectory method as implemented in MOBCAL[65] and were averaged over 100 runs for each conformer. Intensities were derived via a simple Boltzmann analysis and normalized with respect to the lowest-energy conformer. In the majority of cases, both "chair" and "boat" configurations of the proline residue were obtained (following the nomenclature from our previous study on H^+GPGG)[37] and the lower energy conformer was considered to obtain the theoretical intensities. The lower energy "chair" form is shown for *cis*-1r, *cis*-1, and *trans* species in the figures to provide accurate comparison of bond lengths. The *cis*-2r structures unilaterally prefer "boat" over "chair", so the boat form is shown for this conformer in the figures. The differences in hydrogen bond lengths and intensities are relatively minor between "chair" and "boat" conformers, but to reproduce our results exactly, this additional structural feature must be taken into account.

Hydrogen bonds were verified and quantified using the Quantum Theory of Atoms in Molecules (QTAIM) as implemented in the Multiwfn computational chemistry package[66] with the CAM-B3LYP-D3BJ/6-311++G(d,p) densities. The Poincaré−Hopf theorem was found to hold in every case; this fulfills a necessary condition for all critical points to be found, ensuring no interaction is missed. Hydrogen bonds were verified to exist by three criteria: viz., the bond path, the density at the bond critical point (bcp), and the Laplacian at the bcp. Only bond paths linking a hydrogen to either a nitrogen or oxygen were recognized as hydrogen bonds, and other interactions were treated as weak interactions beyond the scope of this study. Only bond paths with bcp charge densities within the window of 0.002−0.034 au and bcp Laplacians within the window of 0.024−0.139 au were considered hydrogen bonds, in accordance with parameters defined by Koch and Popelier.[50] To assess the relative strengths of hydrogen bonds, the potential energy density, V(r), at the bcp was used. While results on experimental electron densities have led to a relationship between hydrogen bond energies and the value of V(r),[49] we report the raw V(r) value at the bcp and speak in ratios of potential energy densities to assess relative hydrogen bond strengths. We do this to make our results as universal and transferable to other systems as possible. All potential energy densities, charge densities, and Laplacians for all hydrogen bonds in each conformer for each peptide can be found in the Supporting Information.

DOI: 10.1021/acs.jpcb.9b03803
J. Phys. Chem. B 2019, 123, 5730−5741

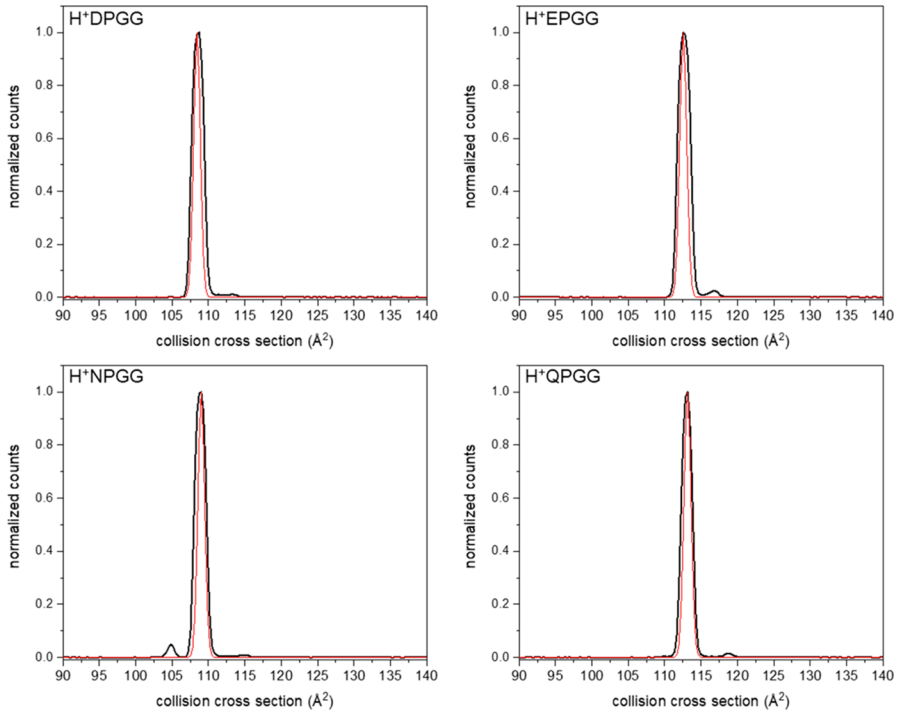

Figure 1. Collision cross section distributions for singly protonated DPGG, EPGG, NPGG, and QPGG. Red lines show the calculated peak width expected for a single conformation.

2.2. Experimental Details. DPGG, NPGG, EPGG, and QPGG were synthesized through standard Fmoc solid-phase peptide synthesis using Fmoc-protected amino acids and Fmoc-Gly-Wang resin (Midwest Biotech, Fishers, IN). Deprotection was performed with 20% piperidine in dimethylformamide and 1,3-diisopropylcarbodiimide/6-chloro-1-hydroxybenzotriazole were used as the coupling reagents. Peptides were cleaved from the resin using an 18:1:1 ratio of trifluoracetic acid:triisopropylsilane:methanol. Peptides were precipitated into, and washed using, ice-cold ether and then dried and used without further purification. Purity was estimated to be >90% by MS analysis.

Electrospray solutions were prepared to ~10 μM in 50/50 water/methanol. IMS theory[65,67−69] and instrumentation[70] are provided in detail elsewhere. Briefly, ions were produced by electrospray ionization (Triversa Nanomate autosampler, Advion, Ithica, NY) and then transferred and stored in an ion funnel trap at the entrance to the IMS-MS instrument.[70,71] The gate is periodically opened for ~75 μs to release ion packets into the 3-m drift tube filled with 3.00 ± 0.03 Torr He buffer gas, held at ~10 V cm^{-1}. The shapes of ions are first determined by measuring the time required to traverse the drift tube (t_d). Using Equation 1, the drift time can be related to the collision cross section Ω,[29,65,72,73]

$$\Omega = \frac{(18\pi)^{1/2}}{16}\frac{ze}{(k_B T)^{1/2}}\left[\frac{1}{m_I}+\frac{1}{m_B}\right]^{1/2}\frac{t_D E}{L}\frac{760}{P}\frac{273}{T}\frac{1}{N} \quad (1)$$

ze is the charge on the ion, E is the electric field, L is the length of the drift tube, P and T are the gas pressure and temperature, and N is the neutral number density of the buffer gas (at STP). m_I and m_B are the masses of the ion and buffer gas, respectively. Structures with large collision cross sections (CCS) interact with the buffer gas more than compact species, resulting in a difference in drift time (t_D) through the IMS cell as compared to ions with compact CCSs. Mobility-separated ions elute from the drift tube and are pulsed orthogonally into a time-of-flight mass spectrometer for analysis of their mass-to-charge (m/z) ratios. While other studies have focused on gently handling ions upon storage, this study sought to characterize the optimal hydrogen bonding pattern in the absence of solvent. Therefore, we have optimized the ion storage conditions to reflect the gas-phase quasi-equilibrium distributions.[74] Theoretical IMS peak shapes were calculated using the transport eq (eq 2) assuming no loss of ions through chemical reaction ($\alpha = 0$), with further details available in the cited text.[67]

$$\Phi(0, z, t) = \frac{sae^{-\alpha t}}{4(\pi D_L t)^{1/2}}\left(v_d + \frac{z}{t}\right) \times \left[1 - \exp\left(-\frac{r_0^2}{4D_T t}\right)\right] \exp\left[\frac{-(z - v_d t)^2}{4D_L t}\right] \quad (2)$$

3. RESULTS AND DISCUSSION

3.1. Ion Mobility Spectra and Collision Cross Sections. Figure 1 shows the experimental IMS distributions for H$^+$DPGG, H$^+$EPGG, H$^+$NPGG, and H$^+$QPGG. A major peak dominates each CCS distribution alongside minor features (vide infra). In all cases, the theoretical peak shape is a close match to experiment—the slight deviation between the experimental and theoretical peak widths may be due to differences in ion starting positions in the ion storage region or closely related conformations with similar gas-phase collision cross sections. To examine the latter possibility in more detail, we performed quantum chemical calculations informed by our previous benchmark study on the ion mobility spectrum of H$^+$GPGG (see Methods for details). In our previous study, the spectrum was dominated by two *cis* conformers (labeled *cis*-1

DOI: 10.1021/acs.jpcb.9b03803
J. Phys. Chem. B 2019, 123, 5730−5741

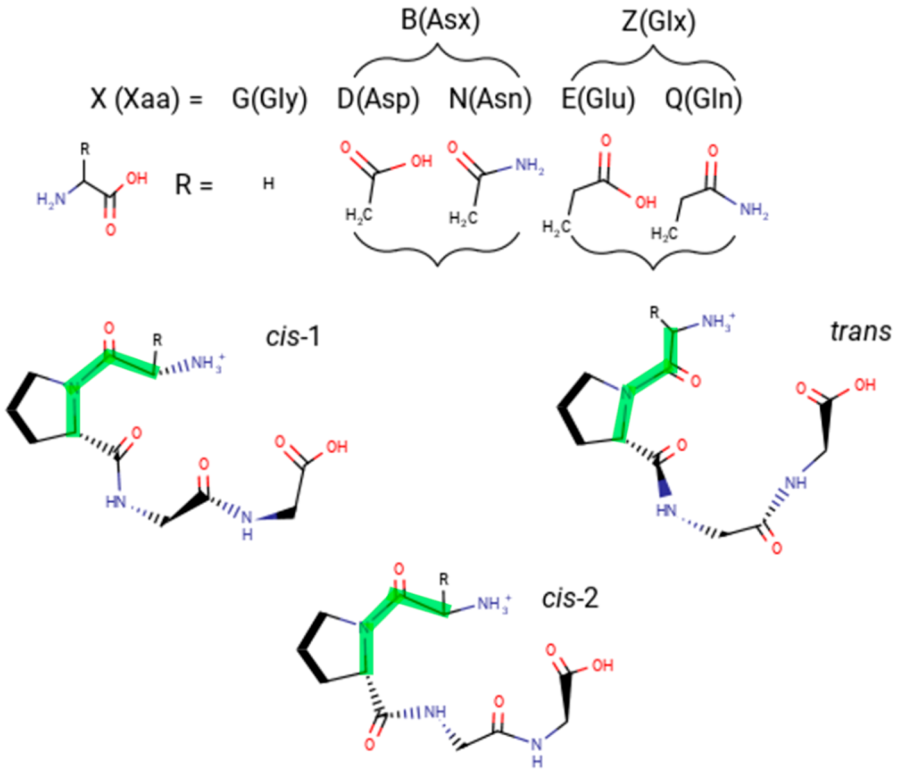

Figure 2. Schematics of the studied H^+XPGG peptides, detailing the differences in the Xaa R groups. The major *trans* conformer and both major *cis* conformers, excepting those with direct involvement of the Xaa R group, are shown with a green line illustrating the *cis* or *trans* orientation about the Xaa−Pro peptide bond.

Table 1. Experimental and Theoretical IMS Collision Cross Sections and Intensities of H^+XPGG (%)[a]

peak	conformer	exptl CCS	theory CCS	exptl %	ΔE_0 %	ΔG %
DPGG -	cis-2r	-	106.8	-	1.8%	2.5%
DPGG 1	cis-1r	108.7	109.0	100%	100%	100%
DPGG 2	cis-1	113.1	112.9	1.3%	1.5%	12.1%
NPGG 1	cis-2r	104.9	107.4	4.9%	5.6%	5.8%
NPGG 2	cis-1r	109.0	108.9	100%	100%	100%
NPGG 3	cis-1	114.6	113.5	1.0%	0.1%	1.8%
EPGG 1	cis-2r	112.6	110.5	100%	100%	23.4%
EPGG 1	cis-1r	112.6	111.1		73.3%	100%
EPGG 2	cis-1	117.0	117.4	2.5%	5.8%	20.2%
QPGG 1	cis-2r	113.1	111.2	100%	100%	100%
QPGG 1	cis-1r	113.1	113.0		17.0%	40.3%
QPGG 2	cis-1	118.5	118.3	1.5%	0.1%	3.9%

[a] ΔE_0 refers to intensities derived from zero-point corrected energies, relative to the lowest energy conformer, ΔG refers to relative intensities derived from the Gibbs free energy. CCS in Å^2.

and *cis*-2) and a single *trans* conformer, with *cis* and *trans* referring to the configuration about the Xaa−Pro peptide bond (Xaa being Gly in the case of GPGG and *cis* vs *trans* convention as illustrated in Figure 2).

Our previous work emphasized the importance of Gibbs free energies in the calculation of the intensity difference between *cis* and *trans* conformers. However, here we find all conformers constituting the experimental spectra are in the *cis* configuration about the Xaa−Pro peptide bond, considerably decreasing the differential effect of the entropic contributions to the free energies (Table 1).[37] We report the intensities derived from both zero-point corrected electronic energies and Gibbs free energies, with relative energies, enthalpies, and Gibbs free energies reported in the Supporting Information.

Table 1 details the experimental collision cross sections for each peak seen in Figure 1 as well as the theoretically obtained collision cross section for each assigned conformer. It is readily apparent that theory agrees well with experiment, with the largest deviations occurring in minor, broad features and all within 3% of the experimental CCS. The dominant peaks of H^+DPGG and H^+NPGG are also extraordinarily similar (within 0.3 Å^2 experimentally, 0.1 Å^2 according to theory)

DOI: 10.1021/acs.jpcb.9b03803
J. Phys. Chem. B 2019, 123, 5730−5741

indicating similar low-lying conformers between the two peptides. The dominant conformers of H^+EPGG and H^+QPGG present larger cross sections than their counterparts (H^+DPGG and H^+NPGG, respectively), which is expected due to the extra methylene bridge. Here we refer to conformers wherein the Xaa R group (as shown in Figure 2) interacts with the C-terminal residue as either *cis*-1r or *cis*-2r, depending on the orientation of the backbone (these structures can be seen in more detail in Figures 6 and 7, vide infra). In Table 1, *cis*-1 refers to the conformer with a *cis*-1 backbone wherein the Xaa R group interacts only with the N-terminus, forming a hydrogen bond with the ammonium group (structure for each peptide available in the Supporting Information, H^+QPGG structure in Figure 8). It should be noted that while *cis*-2 conformers were obtained computationally, they are higher in energy than the *cis*-1 conformers and do not contribute to the experimental spectrum, unlike *cis*-2r. This is expected, as the *cis*-2 conformer in GPGG is higher in energy than both the *trans* and *cis*-1 species.[37]

What is unexpected, however, is that *cis*-2r makes up the major peak of H^+QPGG and H^+EPGG (when considering electronic energies in the case of H^+EPGG), rather than *cis*-1r as in the case of H^+DPGG and H^+NPGG. Both species, *cis*-2r and *cis*-1r, are coincident in collision cross section and not resolved in the experimental spectra of H^+EPGG and H^+QPGG. This is interesting as the H^+DPGG peak is either unresolved or undetected in the experimental spectrum, and the H^+NPGG *cis*-2r conformer makes up a minor peak lower in CCS than the major peak. The ordering of theoretical cross sections allows us to assign visible peaks (as in H^+NPGG); however, the error in the collision cross sections (reported to be 3%)[75] is large enough for the H^+DPGG, H^+EPGG, and H^+QPGG peaks to fall within experimental resolution. The H^+NPGG *cis*-2r peak falls within error of the main peak as well; however, the presence of an additional experimental peak, for which the *cis*-2r theoretical cross section is *also* within resolution of, warrants assignment to this minor peak. Additionally, the intensities of the minor H^+NPGG peak and the *cis*-2r conformer are close enough to assign *cis*-2r to the minor peak. As the *cis*-2r conformer increases in cross section from H^+DPGG to H^+NPGG and H^+EPGG to H^+QPGG, this makes us confident in noting that the H^+DPGG peak is likely simply too minute to be detected in the spectrum and, in H^+EPGG and H^+QPGG, *cis*-2r becomes coincident with *cis*-1r.

3.2. Validation of QTAIM Approach. Only hydrogen bonds vetted by QTAIM analysis (as described in Methods) are described for each conformer. We will primarily consider the potential energy densities at bond critical points and H···A distances (where A refers to a hydrogen bond acceptor) to determine hydrogen bond strength. We do this, rather than reporting D···A distances (where D refers to a hydrogen bond donor), mainly because while hydrogen bond distances are a major factor in determining their strength, the angle between the donor, hydrogen, and acceptor is also a major component in assessing hydrogen bond strengths, and this information is encoded in the H···D distances more so than in the D···A distances, allowing us to discuss a large amount of interactions more readily.[76] While D···A distances are the preference when considering crystal structures due to the decreased variance in length,[16] this restriction does not apply to computations which are all performed in the same manner, allowing us more fidelity in assessing relative interaction strengths.

Before we analyze the abundance of each conformer, we need a measure of the relative strengths of hydrogen bonds. Figure 3 shows the correlation between hydrogen bond lengths

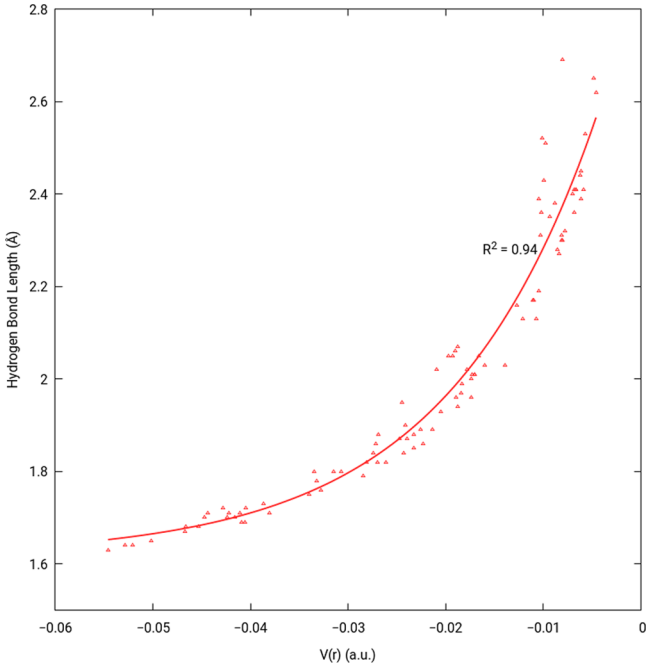

Figure 3. Hydrogen bond length vs potential energy density at the bcp for every hydrogen bond in every conformer and peptide evaluated in this study. R^2 coefficient displayed for exponential fit.

and potential energy densities at the bond critical point by plotting these values with an exponential fit. The coefficient of determination (R^2) of the exponential fit is 0.94, indicating an impressive correlation between bond lengths and the evaluated potential energy densities. Throughout this paper, we will discuss ratios of the potential energy density to indicate improvement or degradation of hydrogen bonding strength between conformers. This is inspired by previous work relating the bond critical point potential energy density to hydrogen bond strengths in a linear fashion.[49] While the fit between hydrogen bond lengths, considered to be an indirect indicator of hydrogen bond strength, and the potential energy densities is exponential, it is clear that a linear correlation exists when omitting the weakest hydrogen bonds. The exponential behavior exhibited in Figure 3 is a product of including a large range of hydrogen bond lengths (>1 Å).

3.3. The Absence of *trans* Conformers. Before exploring the intricacies of the various *cis* conformers, it would be prudent to begin discussion by addressing the most striking difference from the previous work on H^+GPGG: the absence of *trans* conformers in the experimental spectra for H^+XPGG. Table 2 details the zero-point corrected electronic energy and Gibbs free energy differences between the lowest energy *trans* conformer and lowest energy *cis* conformer of protonated forms of H^+GPGG, H^+DPGG, H^+NPGG, H^+EPGG, and H^+QPGG. Aside from H^+GPGG, the Gibbs free-energy-derived relative intensities are less than 0.3% for all H^+XPGG species presented here. There is a large shift in the *trans*/*cis* relative energies (by 3 kcal/mol or more favoring *cis*) on going from H^+GPGG to H^+XPGG. Our analysis (vide infra) suggests that *trans* is disfavored because of its restricting

DOI: 10.1021/acs.jpcb.9b03803
J. Phys. Chem. B 2019, 123, 5730−5741

Table 2. Theoretical Collision Cross Sections and Relative Thermochemical Quantities of H⁺XPGG *trans* Conformers (kcal/mol)[a]

peptide	theory CCS	ΔE_0	ΔG	ΔG %
GPGG	94.9	−0.517	0.834	24.47%
DPGG	108.7	3.141	3.474	0.28%
NPGG	109.8	4.339	4.410	0.06%
EPGG	113.2	2.885	3.749	0.18%
QPGG	114.2	4.611	4.337	0.07%

[a] ΔE_0 refers to the zero-point corrected energies, relative to the lowest energy protonated cis conformer while ΔG to Gibbs free energies. CCS in Å^2.

backbone limiting hydrogen bonding in H⁺XPGG compared to the *cis* species.

Figure 4 presents the *trans* conformers of H⁺XPGG in comparison to the *trans* conformer of H⁺GPGG, with blue, dashed interactions representing interactions changing by 0.05 Å or more from peptide to peptide (e.g., blue interactions in H⁺NPGG (Figure 4C) are changed by 0.05 Å or more relative to H⁺DPGG). At first glance, the lowest energy *trans* conformers presented in Figure 4 seem to be functionally identical. However, the structural orientation in the trans isomer does not allow favorable interactions of the −R group with the C-terminus without significant strain. In particular, introducing the carbonyl-containing N-terminal peptide induces a twist of the N-terminus when compared to GPGG. Comparing GPGG to DPGG (Figure 4A,B), the dihedral angle between the C-terminal carbonyl carbon, α carbon, nitrogen, and hydrogen changes by almost 17°, and this twist increases to nearly 24° when comparing to EPGG. Whereas the GPGG *trans* species features two N-terminal hydrogen bonds, one with the C-terminus and another with the N-terminal carbonyl, the other XPGG species severely weaken the second interaction.

Aside from the loss of this interaction and the gain of a weak CH···O interaction, the progression from D to N to E to Q has one consistent trend of magnitude: the gradual strengthening of the N-terminal hydrogen bond with the Xaa R group carbonyl. In H⁺DPGG (Figure 4B), this new hydrogen bond has a length of 2.02 Å, which decreases to 1.88 Å upon substitution of D with N (Figure 4C), indicating a significant strengthening of this interaction. This strengthening is expected, as the carbonyl group of a carboxamide is more polar and a better hydrogen acceptor than the carbonyl group of a carboxylic acid. Similarly, when comparing H⁺EPGG to H⁺QPGG (Figure 4D to Figure 4E), the N-terminal hydrogen bond decreases by 0.12 Å, indicating strengthening as the carboxylic acid group is replaced with a carboxamide group. Both H⁺EPGG and H⁺QPGG contain a stronger N-terminal interaction with the Xaa R group than their counterparts, a strengthening associated with the extra flexibility afforded by the additional methylene bridge. This behavior establishes a clear pattern: interactions with the Xaa R group are strengthened upon substitution of a carboxylic acid group with a carboxamide group (D to N or E to Q) and upon addition of a methylene bridge (D to E or N to Q). However, similar trends are also present for the *cis* conformers (vide infra); hence, the relative effects between *trans* and *cis* have to be analyzed.

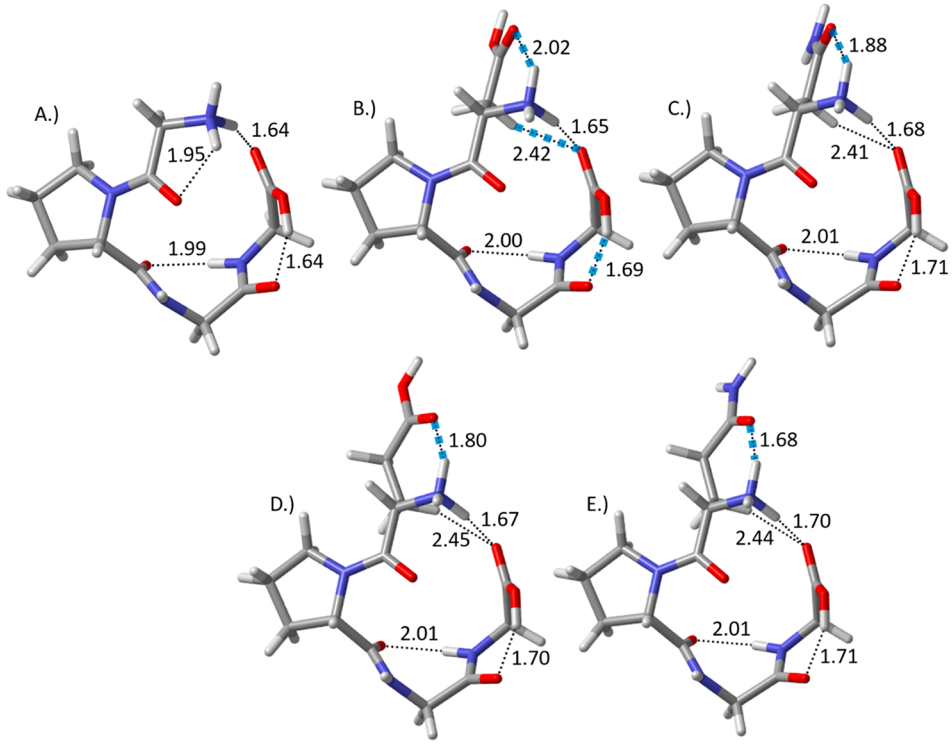

Figure 4. H⁺XPGG *trans* conformers absent from experimental spectra with hydrogen bond distances (Angstroms). A−E show the dominant *trans* conformers of H⁺GPGG, H⁺DPGG, H⁺NPGG, H⁺EPGG, and H⁺QPGG, respectively. Potential interaction distances are given where relevant (vide supra) with blue, dashed interactions representing distance changes of 0.05 Å or more from the previous peptide (e.g., from A to B, B to C, etc.) while red, dashed interactions mark distance changes of 0.05 Å or more only when comparing a ZPGG conformer to the associated BPGG conformer (i.e., EPGG to DPGG or QPGG to NPGG).

DOI: 10.1021/acs.jpcb.9b03803
J. Phys. Chem. B 2019, 123, 5730−5741

Figure 5 plots the sum of the bcp potential energy densities of each hydrogen bond in *trans* minus the total potential energy density of every hydrogen bond in the conformer referred to as *cis*-1r (vide infra), a quantity we will refer to as ΔV(r). ΔV(r) is plotted with the zero-point corrected electronic energy difference between *trans* and *cis*-1r (ΔE_0). Here we use *cis*-1r as an example, but a similar trend exists for *cis*-2r when compared to *trans*. ΔV(r) correlates extremely well with ΔE_0 (R^2 = 0.95), and it is clear that *trans* is favored in terms of pure hydrogen bonding strength. However, the strong correlation between ΔE_0 and ΔV(r) indicates that as the *cis*-1r/*trans* hydrogen bonding strength gap closes, *trans* becomes increasingly disfavored. This trend can also be seen in the enthalpy and Gibbs free energy differences, though the correlation degrades slightly as ΔV(r) is purely an electronic quantity and thermochemical properties will correspond with it only as well as the underlying electronic component.

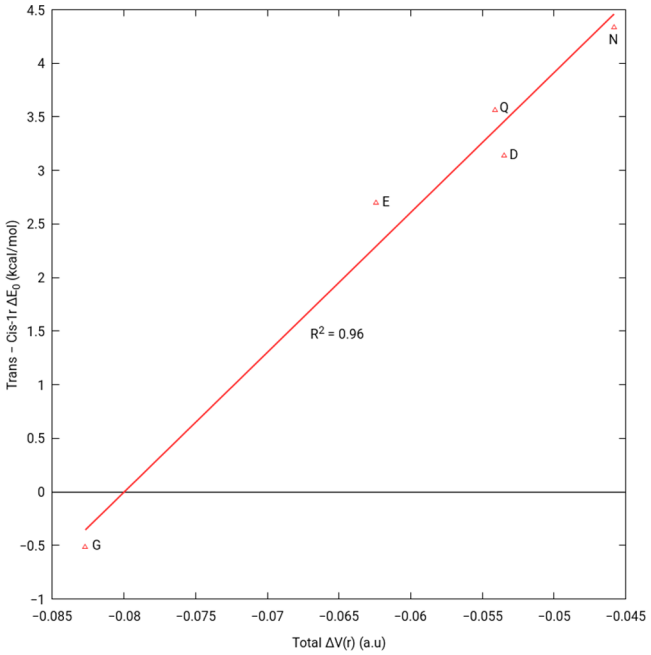

Figure 5. Zero-point corrected electronic energy differences of *trans* − *cis*-1r vs differences in total hydrogen bond potential energy densities, evaluated at the bcp. Each point labeled with the "X" residue of H$^+$XPGG. R^2 displayed for linear fit.

The trend present in Figure 5 is evident when considering H$^+$GPGG, H$^+$DPGG, and H$^+$NPGG. ΔV(r) shifts from −0.0827 au in H$^+$GPGG to −0.0535 au in H$^+$DPGG, a decrease of 35%. It is the addition of new hydrogen bonds in *trans* and *cis*-1r that causes H$^+$GPGG and H$^+$DPGG to differ so much in terms of the relative population of conformers. The *cis*-1r specimen is able to form bifurcated hydrogen bonds (vide infra) which sum to be stronger than the isolated hydrogen bond the *trans* specimen is able to form between the protonated N-terminus and the new Xaa side chain carbonyl group. This is further validated when comparing H$^+$DPGG and H$^+$NPGG: *cis*-1r is able to see a greater change in the strength of its hydrogen bonding network than *trans*, further widening the energy gap, though not to as large a degree as forming the hydrogen bonds in the first place. H$^+$EPGG and H$^+$QPGG follow the same overall trend as H$^+$DPGG and H$^+$NPGG, with a decrease in ΔV(r) corresponding to an increase in ΔE_0. Next, we analyze the more complicated case of the two dominant *cis* conformers to explore how their hydrogen bond networks evolve upon mutation and what advantages and disadvantages hydrogen bond coupling can confer.

3.4. HXH Coupling Varies Depending on Mutation.

The lowest Gibbs free energy conformer of H$^+$DPGG, H$^+$NPGG, and H$^+$EPGG is referred to as *cis*-1r. Here, *cis* refers to a *cis* orientation about the Pro−Xaa peptide bond, the -1 refers to the same skeletal structure as the lowest-lying *cis* conformer of H$^+$GPGG, and the "r" denotes an interaction between the R group of the Xaa residue and the C-terminus. The carbonyl of the Xaa R group in *cis*-1r accepts two hydrogen bonds (Figure 6B−E): one from the protonated N-

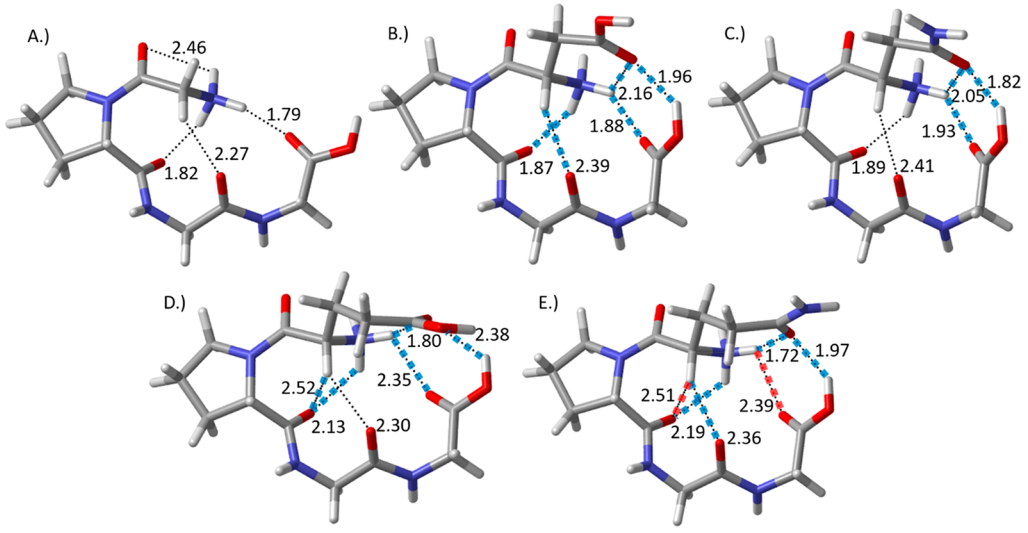

Figure 6. H$^+$XPGG *cis*-1r conformers found in experimental spectra and relevant distances (Å). A−E show the *cis*-1 conformer H$^+$GPGG and the *cis*-1r conformers of H$^+$DPGG, H$^+$NPGG, H$^+$EPGG, and H$^+$QPGG, respectively. Potential interaction distances are given where QTAIM analysis determined a hydrogen bond to exist (vide supra) with blue, dashed interactions representing distance changes of 0.05 Å or more from the previous peptide (e.g from A to B, B to C, etc.), while red, dashed interactions mark distance changes of 0.05 Å or more only when comparing a ZPGG conformer to the associated BPGG conformer (i.e., EPGG to DPGG or QPGG to NPGG).

DOI: 10.1021/acs.jpcb.9b03803
J. Phys. Chem. B 2019, 123, 5730−5741

terminus and one from the hydroxyl group of the C-terminus. Figure 6 presents *cis*-1r of H^+XPGG in comparison to the *cis*-1 conformer of H^+GPGG.

Considering the H^+GPGG *cis*-1 conformer as a control, the H^+DPGG *cis*-1r conformer contains two new hydrogen bonds compared to H^+GPGG and lengthens the three remaining hydrogen bonds. The N-terminal hydrogen bond with the Xaa carbonyl group is now absent, the angle and distance becoming unfavorable as the new bifurcated hydrogen bonds with the Xaa carbonyl are formed. Bifurcated hydrogen bonds of the nature seen in *cis*-1r can be referred to as HXH bonds, one acceptor split by two donors.[77] These types of bifurcated hydrogen bonds, in flexible, biorelevant systems, have been shown to have negative cooperativity (i.e., the addition of one hydrogen bond weakens the other); however, the sum of the interaction energies typically eclipses that of a single hydrogen bond alone.[78,79] Recently, the coupling of hydrogen bond lengths in HXH systems has been explored experimentally and computationally in the active sites of ketosteroid isomerase and photoactive yellow protein, establishing the importance of these couplings in biological systems.[16] Taking this a step further, our computational investigation of tetrapeptide secondary structure explores whether an empirical rule can be derived that determines the relationship between the HXH interaction distances as the acceptor (i.e., the Xaa residue) is varied.

Substituting aspartic acid with asparagine has the effect of making the Xaa R group carbonyl a better hydrogen bond acceptor. The strengthening of both Xaa R group carbonyl hydrogen bonds is the most significant change when comparing all lowest-lying conformers of D H^+PGG and H^+NPGG (Figures 3, 6, and 7). Taking the *cis*-1r conformer as an example, only three of the distances labeled in Figure 6 differ by 0.05 Å or more between H^+DPGG and H^+NPGG: the two hydrogen bonds with the Xaa R group carbonyl and the hydrogen bond between the N-terminus and C-terminal carbonyl. The HXH Asp carbonyl hydrogen bonds are both over 0.1 Å longer than the Asn interactions, indicating a strengthening of both interactions in Asn due to the more electronegative carbonyl. This effect is also observed when substituting Glu with Gln: both hydrogen bonds with the Xaa R group carbonyl shorten by over 0.05 Å.

Interestingly, there is a coupling between these Xaa R group carbonyl hydrogen bonds and the hydrogen bond between the same N-terminal hydrogen and the C-terminal carbonyl. This hydrogen bond increases in length by 0.05 Å, indicating a weakening of this interaction as the R group carbonyl interaction is favored. This negative coupling is mimicked when substituting Glu with Gln, indicating that the changes in the hydrogen bond network around the Xaa R group carbonyl are unaffected by the extra methylene bridge in Glu and Gln. Similar strengthening of the R group carbonyl interactions upon substitution of Asp with Asn can be seen in *cis*-1 and *cis*-2r (vide infra). However, in *cis*-2r, the CH···O hydrogen bond with the Xaa side chain also shortens by more than 0.05 Å.

Substituting Asp with Glu leads to a further increase in the Xaa R group carbonyl hydrogen bond strengths due to the extra flexibility afforded by the additional methylene bridge. The *cis*-1r N-terminal ammonium hydrogen bond with the Glu R group carbonyl is 1.80 Å compared with 2.16 Å in H^+DPGG (Figure 6). This effect is primarily due to an improvement of the hydrogen bond angle ($<_{NH\cdots O}$) which increases from 119.7° in H^+DPGG to 153.3° in H^+EPGG. Unlike the transition from H^+DPGG to H^+NPGG, substituting Asp with Glu causes the other Xaa R group carbonyl hydrogen bond (with the C-terminal hydroxyl) to decrease in strength, the interaction increasing in length from 1.96 to 2.38 Å. The lengthening of the C-terminal hydroxyl hydrogen bond in H^+EPGG compared with H^+DPGG is due to the R group carbonyl rotating away from the hydroxyl to optimize the charge-assisted hydrogen bond with the ammonium group. This effect is also seen in comparing H^+NPGG to H^+QPGG, here the carbonyl hydrogen bond with the N-terminus shortens from 2.05 to 1.72 Å and the hydrogen bond with the C-terminal hydroxyl group lengthens from 1.82 to 1.97 Å.

This reciprocal coupling raises an important point: the enhancement of the HXH hydrogen bonds when substituting Asp with Asn or Glu with Gln resulted from the increase of a hydrogen bond acceptor's capacity to accept whereas the enhancement on substitution of Asp with Glu or Asn with Gln resulted from increased flexibility. In fact, the Asp to Asn and Glu to Gln enhancements can be referred to as *radial*, whereas the Asp to Glu and Asn to Gln enhancements can be thought of as *angular*. Radial enhancement leads to the shortening of both HXH hydrogen bonds, whereas angular enhancement causes the strongest (in this case, the charge-assisted hydrogen bond with the N-terminus) of the two hydrogen bonds to be favored. Thus, while broad statements can be made about the coupling in specific hydrogen bond networks, here we show that in an HXH hydrogen bond changing the acceptor residue can result in positive or negative coupling depending on the way the Xaa acceptor is enhanced.

QTAIM results bolster the evidence found from bond length analysis. Figure 8 presents the *cis*-1r, *cis*-2r, *cis*-1, and *trans* conformers of H^+QPGG with each hydrogen bond labeled in groups. Hydrogen bonds **1** and **5** are the two making up the bifurcated system including the Xaa carbonyl group as a donor, with **1** being the interaction with the N-terminus and **5** being the interaction with the C-terminal hydroxyl. Table 3 contains the potential energy densities evaluated at the bond critical point of each bond in both *cis*-1r and *cis*-2r. The substitution of D with N leads to a strengthening of both interactions in both conformers, as expected from length analysis: interaction **1** becomes more favorable by 31% in *cis*-1r and 39% in *cis*-2r, while interaction **5** becomes more favorable by 55% in *cis*-1r and 76% in *cis*-2r. The increase in stability of **1** when substituting E with Q is extremely similar to the increase seen when substituting D with N: 32% in *cis*-1r and 35% in *cis*-2r. This QTAIM analysis confirms the preceding length analysis: in both *cis*-1r and *cis*-2r, substituting a carboxylic acid group with a carboxamide group leads to positive coupling.

Where *cis*-1r and *cis*-2r diverge is in the behavior of substituting Asp with Glu and Asn with Gln. In *cis*-1r, **5**

Table 3. Potential Energy Densities of Hydrogen Bonds 1 and 5 (au)[a]

	cis-1r		cis-2r	
X	1	5	1	5
D	−0.0127	−0.0174	−0.0241	−0.0107
N	−0.0166	−0.0270	−0.0335	−0.0188
E	−0.0307	−0.0088	−0.0332	−0.0139
Q	−0.0405	−0.0184	−0.0447	−0.0214

[a]V(r) evaluated at bond critical points, and hydrogen bonds grouped and labeled according to Figure 8.

DOI: 10.1021/acs.jpcb.9b03803
J. Phys. Chem. B 2019, 123, 5730−5741

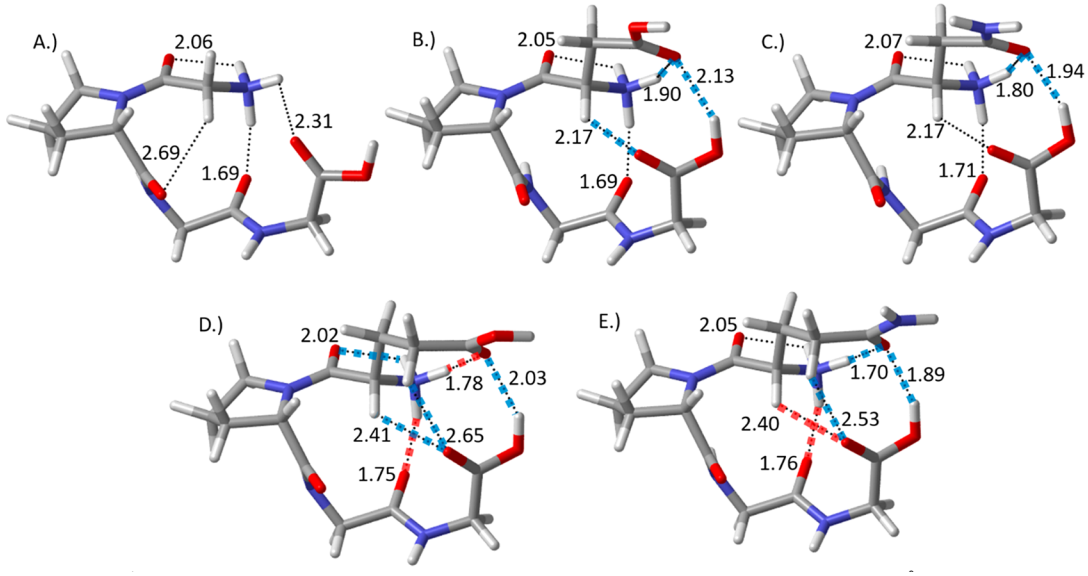

Figure 7. H^+XPGG *cis*-2r conformers found in experimental spectra and relevant distances (Å). A–E show the *cis*-2 conformer H^+GPGG and the *cis*-2r conformers of H^+DPGG, H^+NPGG, H^+EPGG, and H^+QPGG, respectively. Potential interaction distances are given where relevant (vide supra) with blue, dashed interactions representing distance changes of 0.05 Å or more from the previous peptide (e.g from A to B, B to C, etc.), while red, dashed interactions mark distance changes of 0.05 Å or more only when comparing a ZPGG conformer to the associated BPGG conformer (i.e., EPGG to DPGG or QPGG to NPGG).

decreases in magnitude by 49% while seeing an increase in stability (30%) in *cis*-2r. Similarly, when considering the Asn to Gln substitution, *cis*-2r sees two increases in magnitude while **1** increases and **5** decreases in *cis*-1r. The QTAIM analysis of *cis*-2r agrees with changes in the bond lengths (shown in Figure 7); however, now we have the question: why does adding an extra methylene bridge have differing effects in *cis*-1r and *cis*-2r? Additionally, does the disparity between these hydrogen bond network effects explain why *cis*-2r becomes more stable than *cis*-1r in the case of H^+QPGG?

3.5. Slight Differences in Hydrogen Bond Networks Propagate: How *cis*-2r Becomes Preferred. *cis*-2r differs from *cis*-1r by a rotation of the bond between the alpha and carbonyl carbons of proline, thus switching the carbonyl involved in hydrogen bonding with the N-terminus from Pro-2 to Gly-3. This change in the hydrogen bonding network is slight, but interacting with the nearer carbonyl allows a rotation of the N-terminus compared to *cis*-1r. Table 4 presents the potential energy densities of hydrogen bond **2**; **2** being the interaction between the N-terminus and the Pro-2 carbonyl (in *cis*-1r) or the Gly-3 carbonyl (in *cis*-2r). In both *cis*-1r and *cis*-2r, the potential energy of **2** decreases in magnitude as substitution occurs from D to N, D to E, N to Q, and E to Q.

Table 4 also presents the dihedral angle following the carbonyl carbon of Xaa to the hydrogen involved in interaction **2** as a measure of the twisting of the N-terminus. In *cis*-2r, there is only a slight change in the dihedral, with the largest difference being less than 4 degrees. In the case of *cis*-1r, however, substitution of D with E leads to a significant twisting of the N-terminus represented by a dihedral angle change of 16 degrees. This change in the dihedral angle corresponds to a large drop in the magnitude of the potential energy density, 50%, while in *cis*-2r the slight change in dihedral angle only corresponds to a drop of 17%. In *cis*-1r, the trend is consistent: on substitution from D to N to E to Q, the dihedral angle drops continuously as does the strength of the hydrogen bond.

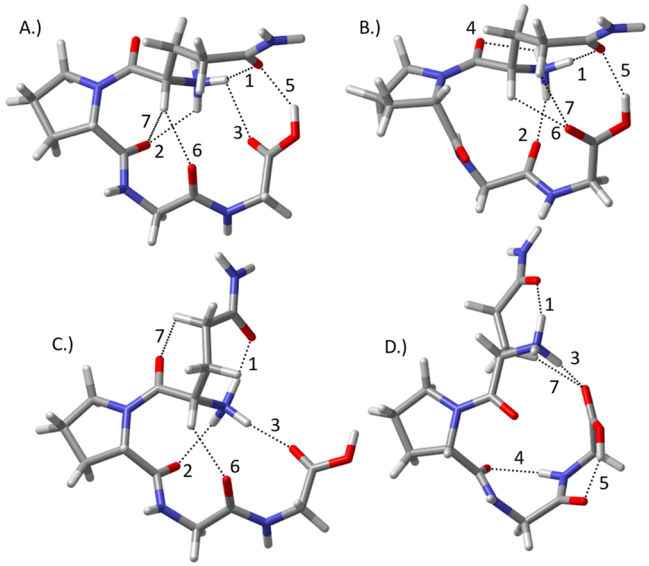

Figure 8. H^+QPGG *cis*-1r, *cis*-2r, *cis*-1, and *trans* conformers, respectively, with hydrogen bonds labeled by group. Groups 1 through 3 contain ammonium group interactions: group 1 with the carbonyl of the Xaa (in this case, Gln) R group, group 2 with either the Pro2 carbonyl or the Gly3 carbonyl (in the case of *cis*-2r), and group 3 with the C-terminal carbonyl. Group 4 contains miscellaneous amine interactions not fitting into the previous groups, group 5 contains hydrogen bonds with the C-terminus acting as a donor, group 6 contains hydrogen bonds with the Xaa α carbon acting as a donor, and group 7 contains miscellaneous hydrogen bonds with CH carbon donors.

Interestingly, the dihedral angles of *cis*-1r and *cis*-2r seem to approach each other upon substitution, with the final difference being less than 3 degrees.

All trends in Table 4 point to a continuous decrease in the strength of interaction **2** as the strength of interaction **1** is increased (Table 3). In both *cis*-2r and *cis*-1r, the greatest

DOI: 10.1021/acs.jpcb.9b03803
J. Phys. Chem. B 2019, 123, 5730–5741

Table 4. Potential Energy Densities of Interaction 2 (au) and Associated Dihedral (deg)[a]

	V(r)		$\theta_{CCN\,H}$	
X	cis-1r	cis-2r	cis-1r	cis-2r
D	−0.0240	−0.0409	−64.0	−87.7
N	−0.0226	−0.0381	−66.1	−88.1
E	−0.0121	−0.0340	−80.0	−85.5
Q	−0.0105	−0.0328	−82.1	−84.9

[a]V(r) evaluated at bond critical points, and hydrogen bonds grouped and labeled according to Figure 8.

change in dihedral angle happens upon substitution of N with E, corresponding with the greatest change in **2**. In the case of *cis*-1r, which possesses a precipitous change in the N-terminal twisting dihedral angle, substitution of N with E also corresponds to the largest increase in the strength of **1**. Clearly, as **1** increases in strength, a twist is induced in the N-terminus of *cis*-1r to optimize the interaction, which corresponds to a decrease in the strength of **2**. *cis*-2r, on the other hand, already has a near optimal dihedral angle characterizing this N-terminal twist due to the proximity of the Gly-3 carbonyl to the N-terminus. This effect causes the decrease in **2** (and the increase in **1**) to be less marked in *cis*-2r than in *cis*-1r, leading to higher magnitudes in interactions **1**, **2**, and **5**. This lack of N-terminal twisting in *cis*-2r also corresponds to the positive coupling seen in the previous section on substitution of D with E and N with Q, as the twisting in *cis*-1r also corresponds to the decrease in the interaction strength of **5**. In the case of **2**, the interaction is only 70% stronger in *cis*-2r than in *cis*-1r in H^+DPGG; however, the hydrogen bond is 212% stronger in H^+QPGG.

Considering the total hydrogen bond potential energy densities, *cis*-2r is favored over *cis*-1r by 27% in H^+DPGG; this quantity is increased to 36% in H^+QPGG, enough to cause *cis*-2r to be favored energetically over *cis*-1r. The increase in **2** corresponds to 43% of this total increase, the largest single increase in hydrogen bonding strength upon substitution of D with Q. The more favorable positioning of hydrogen bond **2** in *cis*-2r is the major factor in *cis*-2r becoming more preferable than *cis*-1r in H^+QPGG by positioning the N-terminus optimally for the D to E and N to Q mutations. Twisting of the N-terminus in *cis*-1r is associated with the weakening of multiple hydrogen bonds, compromising the overall stability of the conformer.

4. CONCLUSIONS

This study deals with the consequences of substituting the N-terminus in H^+XPGG with four different residues to form H^+DPGG, H^+NPGG, H^+EPGG, and H^+QPGG. IMS measurements enable the elucidation of multiple peaks for each species and create a platform for the validation of accurate quantum chemical calculations. Utilizing the techniques developed in our previous work on the computational benchmarking of H^+GPGG, we are able to confidently track the changes in the hydrogen bond networks of these peptides and how they relate to the observed IMS distributions. Not only do we see the intricate coupling of hydrogen bonds in these small peptides but we are able to directly relate changes in the network to the identity of the preferred conformer of each peptide.

The *trans* conformer, typically thought to be coincident with *cis* conformers in Pro-containing species, was found to become increasingly less favored as the Xaa residue was varied, despite a stronger overall hydrogen bond network. Plotting the QTAIM bcp potential energy densities along with the *cis*/*trans* relative energies reveals the disfavoring of *trans* to correlate strongly with decreases in the relative strength of the hydrogen bond network. This correlation follows from the more coupled hydrogen bond network of the *cis* species being able to capitalize on the addition of a new hydrogen bond acceptor more so than the backbone-restricted *trans* species with the new R group oriented only toward the N-terminus. HXH hydrogen bonds were shown to be both positively and negatively coupled, depending on the way in which a new residue enhances a specific hydrogen bond as well as intricacies in the underlying structure of the hydrogen bonding network. The structure of the *cis*-2r hydrogen bond network is shown to allow the N-terminus to be properly rotated for optimal hydrogen bonding upon substitution of D with Q, leading to *cis*-2r becoming the preferred conformer on mutation. From these results we can draw some general observations:

1. Seemingly minor differences in the hydrogen bonding network can lead to large changes upon mutation.
2. The energy differences of even structurally dissimilar (*cis* and *trans*) conformers can be related to the relative strengths of their hydrogen bonding networks.
3. Coupling in bifurcated hydrogen bonds can be variable depending on the way in which the hydrogen bonds are enhanced.
4. QTAIM potential energy densities at the bond critical point are exponentially related to hydrogen bond lengths, marking these as a good indicator of relative hydrogen bond strength.

Above all, these results highlight the importance of coupling quantum chemical computations with experiment when engineering proteins or drug molecules as the evolution of hydrogen bonding networks in peptides will only grow more complex as the peptide increases in size, belying any simple empirical rule.

■ ASSOCIATED CONTENT

Supporting Information

The Supporting Information is available free of charge on the ACS Publications website at DOI: 10.1021/acs.jpcb.9b03803.

Coordinates of all discussed species, *cis*-1 structures, relative energies, enthalpies, Gibbs free energies of all *cis* species, Laplacians, charge densities, and potential energy densities of all hydrogen bonds of all conformers of each H^+XPGG (PDF)

■ AUTHOR INFORMATION

Corresponding Author

*E-mail: kraghava@indiana.edu.

ORCID

Daniel Beckett: 0000-0003-4833-2269

David E. Clemmer: 0000-0003-4039-1360

Krishnan Raghavachari: 0000-0003-3275-1426

Notes

The authors declare no competing financial interest.

■ ACKNOWLEDGMENTS

This work was supported in part by funds from the National Science Foundation grant CHE-1665427 (K.R.), the National Institutes of Health grants 5R01GM117207 and

DOI: 10.1021/acs.jpcb.9b03803
J. Phys. Chem. B 2019, 123, 5730−5741

5R01GM121751 (D.E.C.) at Indiana University, and the IU President's Diversity Dissertation Fellowship (D.B.).

REFERENCES

(1) Redfern, O. C.; Dessailly, B.; Orengo, C. A. Exploring the Structure and Function Paradigm. *Curr. Opin. Struct. Biol.* **2008**, *18*, 394−402.

(2) Wright, P. E.; Dyson, H. J. Intrinsically Disordered Proteins in Cellular Signalling and Regulation. *Nat. Rev. Mol. Cell Biol.* **2015**, *16*, 18−29.

(3) Wimberly, B. T.; Brodersen, D. E.; Clemons, W. M., Jr; Morgan-Warren, R. J.; Carter, A. P.; Vonrhein, C.; Hartsch, T.; Ramakrishnan, V. Structure of the 30S Ribosomal Subunit. *Nature* **2000**, *407*, 327−329.

(4) Baldwin, A. J.; Kay, L. E. NMR Spectroscopy Brings Invisible Protein States into Focus. *Nat. Chem. Biol.* **2009**, *5*, 808−814.

(5) Mangione, P. P.; Esposito, G.; Relini, A.; Raimondi, S.; Porcari, R.; Giorgetti, S.; Corazza, A.; Fogolari, F.; Penco, A.; Goto, Y.; et al. Structure, Folding Dynamics, and Amyloidogenesis of D76N β2-Microglobulin: Roles of Shear Flow, Hydrophobic Surfaces, and α-Crystallin. *J. Biol. Chem.* **2013**, *288*, 30917−30930.

(6) Valleix, S.; Gillmore, J. D.; Bridoux, F.; Mangione, P. P.; Dogan, A.; Nedelec, B.; Boimard, M.; Touchard, G.; Goujon, J.-M.; Lacombe, C.; et al. Hereditary Systemic Amyloidosis Due to Asp76Asn Variant β2-Microglobulin. *N. Engl. J. Med.* **2012**, *366*, 2276−2283.

(7) de Rosa, M.; Barbiroli, A.; Giorgetti, S.; Mangione, P. P.; Bolognesi, M.; Ricagno, S. Decoding the Structural Bases of D76N ß2-Microglobulin High Amyloidogenicity through Crystallography and Asn-Scan Mutagenesis. *PLoS One* **2015**, *10*, No. e0144061.

(8) Jeffrey, G. A.; Saenger, W. *Hydrogen Bonding in Biological Structures*; Springer: Berlin, Germany, 1991.

(9) Bowie, J. U. Membrane Protein Folding: How Important Are Hydrogen Bonds? *Curr. Opin. Struct. Biol.* **2011**, *21*, 42−49.

(10) Pace, C. N.; Fu, H.; Lee Fryar, K.; Landua, J.; Trevino, S. R.; Schell, D.; Thurlkill, R. L.; Imura, S.; Scholtz, J. M.; Gajiwala, K.; et al. Contribution of Hydrogen Bonds to Protein Stability. *Protein Sci.* **2014**, *23*, 652−661.

(11) Lorieau, J. L.; Louis, J. M.; Bax, A. The Complete Influenza Hemagglutinin Fusion Domain Adopts a Tight Helical Hairpin Arrangement at the Lipid:Water Interface. *Proc. Natl. Acad. Sci. U. S. A.* **2010**, *107*, 11341−11346.

(12) Horowitz, S.; Trievel, R. C. Carbon-Oxygen Hydrogen Bonding in Biological Structure and Function. *J. Biol. Chem.* **2012**, *287*, 41576−41582.

(13) Nelson, H. C. M.; Finch, J. T.; Luisi, B. F.; Klug, A. The Structure of an Oligo(dA)·Oligo(dT) Tract and Its Biological Implications. *Nature* **1987**, *330*, 221−226.

(14) Lan, T.; McLaughlin, L. W. The Energetic Contribution of a Bifurcated Hydrogen Bond to the Binding of DAPI to dA-dT Rich Sequences of DNA. *J. Am. Chem. Soc.* **2001**, *123*, 2064−2065.

(15) Offenbacher, A. R.; Hu, S.; Poss, E. M.; Carr, C. A. M.; Scouras, A. D.; Prigozhin, D. M.; Iavarone, A. T.; Palla, A.; Alber, T.; Fraser, J. S.; et al. Hydrogen−Deuterium Exchange of Lipoxygenase Uncovers a Relationship Between Distal, Solvent Exposed Protein Motions and the Thermal Activation Barrier for Catalytic Proton-Coupled Electron Tunneling. *ACS Cent. Sci.* **2017**, *3*, 570−579.

(16) Pinney, M. M.; Natarajan, A.; Yabukarski, F.; Sanchez, D. M.; Liu, F.; Liang, R.; Doukov, T.; Schwans, J. P.; Martinez, T. J.; Herschlag, D. Structural Coupling Throughout the Active Site Hydrogen Bond Networks of Ketosteroid Isomerase and Photoactive Yellow Protein. *J. Am. Chem. Soc.* **2018**, *140*, 9827−9843.

(17) Valentine, S. J.; Counterman, A. E.; Hoaglund-Hyzer, C. S.; Clemmer, D. E. Intrinsic Amino Acid Size Parameters from a Series of 113 Lysine-Terminated Tryptic Digest Peptide Ions. *J. Phys. Chem. B* **1999**, *103*, 1203−1207.

(18) Counterman, A. E.; Clemmer, D. E. Volumes of Individual Amino Acid Residues in Gas-Phase Peptide Ions. *J. Am. Chem. Soc.* **1999**, *121*, 4031−4039.

(19) Valentine, S. J.; Counterman, A. E.; Clemmer, D. E. A Database of 660 Peptide Ion Cross Sections: Use of Intrinsic Size Parameters for Bona Fide Predictions of Cross Sections. *J. Am. Soc. Mass Spectrom.* **1999**, *10*, 1188−1211.

(20) Bohrer, B. C.; Merenbloom, S. I.; Koeniger, S. L.; Hilderbrand, A. E.; Clemmer, D. E. Biomolecule Analysis by Ion Mobility Spectrometry. *Annu. Rev. Anal. Chem.* **2008**, *1*, 293−327.

(21) Lanucara, F.; Holman, S. W.; Gray, C. J.; Eyers, C. E. The Power of Ion Mobility-Mass Spectrometry for Structural Characterization and the Study of Conformational Dynamics. *Nat. Chem.* **2014**, *6*, 281.

(22) Kaleta, D. T.; Jarrold, M. F. Helix−Turn−Helix Motifs in Unsolvated Peptides. *J. Am. Chem. Soc.* **2003**, *125*, 7186−7187.

(23) Servage, K. A.; Silveira, J. A.; Fort, K. L.; Russell, D. H. Cryogenic Ion Mobility-Mass Spectrometry: Tracking Ion Structure from Solution to the Gas Phase. *Acc. Chem. Res.* **2016**, *49*, 1421−1428.

(24) Seo, J.; Hoffmann, W.; Warnke, S.; Bowers, M. T.; Pagel, K.; von Helden, G. Retention of Native Protein Structures in the Absence of Solvent: A Coupled Ion Mobility and Spectroscopic Study. *Angew. Chem., Int. Ed.* **2016**, *55*, 14173−14176.

(25) El-Baba, T. J.; Woodall, D. W.; Raab, S. A.; Fuller, D. R.; Laganowsky, A.; Russell, D. H.; Clemmer, D. E. Melting Proteins: Evidence for Multiple Stable Structures upon Thermal Denaturation of Native Ubiquitin from Ion Mobility Spectrometry-Mass Spectrometry Measurements. *J. Am. Chem. Soc.* **2017**, *139*, 6306−6309.

(26) Dixit, S.; Ruotolo, B. T. A Semi-Empirical Framework for Interpreting Traveling Wave Ion Mobility Arrival Time Distributions. *J. Am. Soc. Mass Spectrom.* **2019**, *30*, 956−966.

(27) Do, T. D.; Sangwan, S.; de Almeida, N. E. C.; Ilitchev, A. I.; Giammona, M.; Sawaya, M. R.; Buratto, S. K.; Eisenberg, D. S.; Bowers, M. T. Distal Amyloid β-Protein Fragments Template Amyloid Assembly. *Protein Sci.* **2018**, *27*, 1181−1190.

(28) Beveridge, R.; Migas, L. G.; Kriwacki, R. W.; Barran, P. E. Ion Mobility Mass Spectrometry Measures the Conformational Landscape of p27 and Its Domains and How This Is Modulated upon Interaction with Cdk2/Cyclin A. *Angew. Chem., Int. Ed.* **2019**, *58*, 3114−3118.

(29) Clemmer, D. E.; Jarrold, M. F. Ion Mobility Measurements and Their Applications to Clusters and Biomolecules. *J. Mass Spectrom.* **1997**, *32*, 577−592.

(30) Zhong, Y.; Han, L.; Ruotolo, B. T. Collisional and Coulombic Unfolding of Gas-Phase Proteins: High Correlation to Their Domain Structures in Solution. *Angew. Chem., Int. Ed.* **2014**, *53*, 9209−9212.

(31) Majuta, S. N.; Maleki, H.; Kiani Karanji, A.; Attanyake, K.; Loch, E.; Valentine, S. J. Magnifying Ion Mobility Spectrometry−Mass Spectrometry Measurements for Biomolecular Structure Studies. *Curr. Opin. Chem. Biol.* **2018**, *42*, 101−110.

(32) Zhou, M.; Politis, A.; Davies, R.; Liko, I.; Wu, K.-J.; Stewart, A. G.; Stock, D.; Robinson, C. V. Ion Mobility-Mass Spectrometry of a Rotary ATPase Reveals ATP-Induced Reduction in Conformational Flexibility. *Nat. Chem.* **2014**, *6*, 208−215.

(33) Wyttenbach, T.; Pierson, N. A.; Clemmer, D. E.; Bowers, M. T. Ion Mobility Analysis of Molecular Dynamics. *Annu. Rev. Phys. Chem.* **2014**, *65*, 175−196.

(34) Masson, A.; Kamrath, M. Z.; Perez, M. A. S.; Glover, M. S.; Rothlisberger, U.; Clemmer, D. E.; Rizzo, T. R. Infrared Spectroscopy of Mobility-Selected H+-Gly-Pro-Gly-Gly (GPGG). *J. Am. Soc. Mass Spectrom.* **2015**, *26*, 1444−1454.

(35) Pepin, R.; Petrone, A.; Laszlo, K. J.; Bush, M. F.; Li, X.; Tureček, F. Does Thermal Breathing Affect Collision Cross Sections of Gas-Phase Peptide Ions? An Ab Initio Molecular Dynamics Study. *J. Phys. Chem. Lett.* **2016**, *7*, 2765−2771.

(36) Landreh, M.; Marklund, E. G.; Uzdavinys, P.; Degiacomi, M. T.; Coincon, M.; Gault, J.; Gupta, K.; Liko, I.; Benesch, J. L. P.; Drew, D.; Robinson, C. V. Integrating mass spectrometry with MD simulations reveals the role of lipids in Na+/H+ antiporters. *Nat. Commun.* **2017**, *8*, 13993.

(37) Beckett, D.; El-Baba, T. J.; Clemmer, D. E.; Raghavachari, K. Electronic Energies Are Not Enough: An Ion Mobility-Aided,

DOI: 10.1021/acs.jpcb.9b03803
J. Phys. Chem. B 2019, 123, 5730−5741

Quantum Chemical Benchmark Analysis of H+GPGG Conformers. *J. Chem. Theory Comput.* **2018**, *14*, 5406−5418.
(38) Pepin, R.; Laszlo, K. J.; Marek, A.; Peng, B.; Bush, M. F.; Lavanant, H.; Afonso, C.; Tureček, F. Toward a Rational Design of Highly Folded Peptide Cation Conformations. 3D Gas-Phase Ion Structures and Ion Mobility Characterization. *J. Am. Soc. Mass Spectrom.* **2016**, *27*, 1647−1660.
(39) Bader, R. F. W. Atoms in Molecules. *Acc. Chem. Res.* **1985**, *18*, 9−15.
(40) Bader, R. F. W. *Atoms in Molecules: A Quantum Theory*; Clarendon Press: Oxford, 1990.
(41) Bader, R. F. W. A Quantum Theory of Molecular Structure and Its Applications. *Chem. Rev.* **1991**, *91*, 893−928.
(42) Matta, C. F.; Boyd, R. J. In *The Quantum Theory of Atoms in Molecules: From Solid State to DNA and Drug Design*; Matta, C. F., Boyd, R. J., Eds.; Wiley-VCH: Weinheim, 2007; pp 1−34.
(43) Sanz, P.; Mó, O.; Yáñez, M. Characterization of Intramolecular Hydrogen Bonds and Competitive Chalcogen−Chalcogen Interactions on the Basis of the Topology of the Charge Density. *Phys. Chem. Chem. Phys.* **2003**, *5*, 2942−2947.
(44) Bayat, A.; Fattahi, A. Influence of Remote Intramolecular Hydrogen Bonding on the Acidity of Hydroxy-1,4-Benzoquinonederivatives: A DFT Study. *J. Phys. Org. Chem.* **2019**, *32*, No. e3919.
(45) Martins, M. A. P.; Rodrigues, L. V.; Meyer, A. R.; Frizzo, C. P.; Hörner, M.; Zanatta, N.; Bonacorso, H. G.; Berná, J.; Alajarín, M. Density Functional Theory and Quantum Theory of Atoms in Molecules Analysis: Influence of Intramolecular Interactions on Pirouetting Movement in Tetraalkylsuccinamide[2]rotaxanes. *Cryst. Growth Des.* **2017**, *17*, 5845−5857.
(46) Kumar, P. S. V.; Raghavendra, V.; Subramanian, V. Bader's Theory of Atoms in Molecules (AIM) and Its Applications to Chemical Bonding. *J. Chem. Sci.* **2016**, *128*, 1527−1536.
(47) Espinosa, E.; Molins, E. Retrieving Interaction Potentials from the Topology of the Electron Density Distribution: The Case of Hydrogen Bonds. *J. Chem. Phys.* **2000**, *113*, 5686−5694.
(48) Grabowski, S. J. A New Measure of Hydrogen Bonding Strength − Ab Initio and Atoms in Molecules Studies. *Chem. Phys. Lett.* **2001**, *338*, 361−366.
(49) Espinosa, E.; Molins, E.; Lecomte, C. Hydrogen Bond Strengths Revealed by Topological Analyses of Experimentally Observed Electron Densities. *Chem. Phys. Lett.* **1998**, *285*, 170−173.
(50) Koch, U.; Popelier, P. L. A. Characterization of C-H-O Hydrogen Bonds on the Basis of the Charge Density. *J. Phys. Chem.* **1995**, *99*, 9747−9754.
(51) Sosa, G. L.; Peruchena, N.; Contreras, R. H.; Castro, E. A. Topological Analysis of Hydrogen Bonding Interactions Involving C-H···O bonds. *J. Mol. Struct.: THEOCHEM* **1997**, *401*, 77−85.
(52) Rozas, I.; Alkorta, I.; Elguero, J. Bifurcated Hydrogen Bonds: Three-Centered Interactions. *J. Phys. Chem. A* **1998**, *102*, 9925−9932.
(53) Gilbert, K. *PCMODEL*; Serena Software: Bloomington, IN, 2014.
(54) Halgren, T. A. Merck Molecular Force Field. I. Basis, Form, Scope, Parameterization, and Performance of MMFF94. *J. Comput. Chem.* **1996**, *17*, 490−519.
(55) Stewart, J. J. P. Optimization of Parameters for Semiempirical Methods V: Modification of NDDO Approximations and Application to 70 Elements. *J. Mol. Model.* **2007**, *13*, 1173−1213.
(56) Frisch, M. J.; Trucks, G. W.; Schlegel, H. B.; Scuseria, G. E.; Robb, M. A.; Cheeseman, J. R.; Scalmani, G.; Barone, V.; Petersson, G. A.; Nakatsuji, H.; et al., *Gaussian 16*, Rev. A.01; Gaussian, Inc.: Wallingford, CT, 2016.
(57) Vosko, S. H.; Wilk, L.; Nusair, M. Accurate Spin-Dependent Electron Liquid Correlation Energies for Local Spin Density Calculations: A Critical Analysis. *Can. J. Phys.* **1980**, *58*, 1200−1211.
(58) Lee, C.; Yang, W.; Parr, R. G. Development of the Colle-Salvetti Correlation-Energy Formula into a Functional of the Electron Density. *Phys. Rev. B: Condens. Matter Mater. Phys.* **1988**, *37*, 785−789.
(59) Becke, A. D. Density-Functional Thermochemistry. III. The Role of Exact Exchange. *J. Chem. Phys.* **1993**, *98*, 5648−5652.
(60) Stephens, P. J.; Devlin, F. J.; Chabalowski, C. F.; Frisch, M. J. Ab Initio Calculation of Vibrational Absorption and Circular Dichroism Spectra Using Density Functional Force Fields. *J. Phys. Chem.* **1994**, *98*, 11623−11627.
(61) Yanai, T.; Tew, D. P.; Handy, N. C. A New Hybrid Exchange−Correlation Functional Using the Coulomb-Attenuating Method (CAM-B3LYP). *Chem. Phys. Lett.* **2004**, *393*, 51−57.
(62) Grimme, S.; Antony, J.; Ehrlich, S.; Krieg, H. A Consistent and Accurate Ab Initio Parametrization of Density Functional Dispersion Correction (DFT-D) for the 94 Elements H-Pu. *J. Chem. Phys.* **2010**, *132*, 154104.
(63) Goerigk, L.; Grimme, S. A Thorough Benchmark of Density Functional Methods for General Main Group Thermochemistry, Kinetics, and Noncovalent Interactions. *Phys. Chem. Chem. Phys.* **2011**, *13*, 6670−6688.
(64) Grimme, S.; Ehrlich, S.; Goerigk, L. Effect of the Damping Function in Dispersion Corrected Density Functional Theory. *J. Comput. Chem.* **2011**, *32*, 1456−1465.
(65) Mesleh, M. F.; Hunter, J. M.; Shvartsburg, A. A.; Schatz, G. C.; Jarrold, M. F. Structural Information from Ion Mobility Measurements: Effects of the Long-Range Potential. *J. Phys. Chem.* **1996**, *100*, 16082−16086.
(66) Lu, T.; Chen, F. Multiwfn: A Multifunctional Wavefunction analyzer. *J. Comput. Chem.* **2012**, *33*, 580−592.
(67) Mason, E. A.; McDaniel, E. W. *Transport Properties of Ions in Gases*; John Wiley & Sons, Inc.: New York, NY, 1988; p 90.
(68) Mack, E. Average Cross-Section Areas of Molecules by Gaseous Diffusion Methods. *J. Am. Chem. Soc.* **1925**, *47*, 2468−2482.
(69) Shvartsburg, A. A.; Jarrold, M. F. An Exact Hard-Spheres Scattering Model for the Mobilities of Polyatomic Ions. *Chem. Phys. Lett.* **1996**, *261*, 86−91.
(70) Merenbloom, S. I.; Koeniger, S. L.; Valentine, S. J.; Plasencia, M. D.; Clemmer, D. E. IMS−IMS and IMS−IMS−IMS/MS for Separating Peptide and Protein Fragment Ions. *Anal. Chem.* **2006**, *78*, 2802−2809.
(71) Tang, K.; Shvartsburg, A. A.; Lee, H.-N.; Prior, D. C.; Buschbach, M. A.; Li, F.; Tolmachev, A. V.; Anderson, G. A.; Smith, R. D. High-Sensitivity Ion Mobility Spectrometry/Mass Spectrometry Using Electrodynamic Ion Funnel Interfaces. *Anal. Chem.* **2005**, *77*, 3330−3339.
(72) Wyttenbach, T.; Helden, G. v.; Batka, J. J.; Carlat, D.; Bowers, M. T. Effect of the Long-Range Potential on Ion Mobility Measurements. *J. Am. Soc. Mass Spectrom.* **1997**, *8*, 275−282.
(73) Jarrold, M. F.; Constant, V. A. Silicon Cluster Ions: Evidence for a Structural Transition. *Phys. Rev. Lett.* **1991**, *67*, 2994−2997.
(74) Pierson, N. A.; Valentine, S. J.; Clemmer, D. E. Evidence for a Quasi-Equilibrium Distribution of States for Bradykinin [M + 3H]3+ Ions in the Gas Phase. *J. Phys. Chem. B* **2010**, *114*, 7777−7783.
(75) Siu, C.-K.; Guo, Y.; Saminathan, I. S.; Hopkinson, A. C.; Siu, K. W. M. Optimization of Parameters Used in Algorithms of Ion-Mobility Calculation for Conformational Analyses. *J. Phys. Chem. B* **2010**, *114*, 1204−1212.
(76) Jeffrey, G. A. *An Introduction to Hydrogen Bonding*; Oxford University Press: New York, NY, 1997.
(77) Yang, J.; Gellman, S. H. Energetic Superiority of Two-Center Hydrogen Bonding Relative to Three-Center Hydrogen Bonding in a Model System. *J. Am. Chem. Soc.* **1998**, *120*, 9090−9091.
(78) Yang, J.; Christianson, L. A.; Gellman, S. H. Comparison of an HXH Three-Center Hydrogen Bond with Alternative Two-Center Hydrogen Bonds in a Model System. *Org. Lett.* **1999**, *1*, 11−14.
(79) Parra, R. D.; Furukawa, M.; Gong, B.; Zeng, X. C. Energetics and Cooperativity in Three-Center Hydrogen Bonding Interactions. I. Diacetamide-X Dimers (X = HCN, CH3OH). *J. Chem. Phys.* **2001**, *115*, 6030−6035.

DOI: 10.1021/acs.jpcb.9b03803
J. Phys. Chem. B 2019, 123, 5730−5741